Different escape modes in two-photon double ionization of helium

A. S. Kheifets* and A. I. Ivanov
Research School of Physical Sciences, The Australian National University, Canberra ACT 0200, Australia

I. Bray†
ARC Centre for Matter-Antimatter Studies, Murdoch University, Perth, 6150 Australia

(Received 12 June 2006; published 26 February 2007)

The quadrupole channel of two-photon double ionization of He exhibits two distinctly different modes of correlated motion of the photoelectron pair. The kinematics of the mode associated with the center-of-mass motion favors large total momenta maximized at parallel emission where the interelectron repulsion is strong. In contrast, the mode associated with the relative motion favors large relative momenta maximized at antiparallel emission where the interelectron repulsion is relatively weak. This difference in the interelectron repulsion allows for much wider angular correlation width in the relative motion mode as compared to the center-of-mass mode.

DOI: 10.1103/PhysRevA.75.024702 PACS number(s): 32.80.Fb, 32.80.Rm, 42.50.Hz

The process of correlated motion of multiple ionization fragments has been at the forefront of atomic collision physics during the past decade. Recent progress in experimental techniques made it possible to detect simultaneously a large number of charged reaction fragments with fully determined kinematics [1]. The long-range Coulomb interaction between these fragments makes a full theoretical description of such a process a highly challenging task. In the meantime, the simplest multiple-fragmentation reaction, the single-photon double ionization (SPDI) of helium, is now well understood with accurate theoretical predictions being confirmed experimentally under a wide range of kinematical conditions [2–4]. All the information about the correlated motion of the photoelectrons is described in SPDI by a pair of symmetrized amplitudes $f^{\pm}(\theta_{12},E_1,E_2)$ which depend on the relative interelectron angle and energy [5,6]. The dipole matrix element of SPDI is expressed via these amplitudes as

$$D=\boldsymbol{A}_1\cdot\hat{\boldsymbol{e}}=[f^{+}(\hat{\boldsymbol{k}}_1+\hat{\boldsymbol{k}}_2)+f^{-}(\hat{\boldsymbol{k}}_1-\hat{\boldsymbol{k}}_2)]\cdot\hat{\boldsymbol{e}}. \tag{1}$$

Here $\hat{\boldsymbol{e}}$ is the polarization vector of light and $\hat{\boldsymbol{k}}_i=\boldsymbol{k}_i/k_i$, $i=1,2$, are the unit vectors directed along the photoelectron momenta $\boldsymbol{k}_i$. Under the equal-energy-sharing condition, the antisymmetric amplitude vanishes $f^{-}(E_1=E_2)=0$ and all the information about the SPDI process is contained in one symmetric amplitude f^{+}. Following predictions of the Wannier-type theories [7,8], the SDPI amplitude can be written using the Gaussian ansatz

$$|f^{+}|^2\propto\exp\left[-4\ln 2\frac{(\pi-\theta_{12})^2}{\Delta\theta_{12}^2}\right], \tag{2}$$

where the width parameter $\Delta\theta_{12}$ indicates the strength of angular correlation in the two-electron continuum. Although the analytical theories [7,8] validate Eq. (2) only near the double-ionization threshold, numerical models [9] and direct measurements [10,11] support its validity in a far wider photon energy range.

Two-photon double ionization (TPDI) of He is a much more complex fragmentation process with two competing decay channels into the S and D two-electron continua. In analogy with Eq. (1), the TPDI matrix element can be written as

$$M+Q=\boldsymbol{A}_0\cdot\{\hat{\boldsymbol{e}}\otimes\hat{\boldsymbol{e}}\}_0+\boldsymbol{A}_2\cdot\{\hat{\boldsymbol{e}}\otimes\hat{\boldsymbol{e}}\}_2, \tag{3}$$

where the second-rank tensor $\boldsymbol{A}_2$ represents the quadrupole TPDI amplitude and allows for the following parametrization [12]:

$$\boldsymbol{A}_2=g^{+}[\{\hat{\boldsymbol{k}}_1\otimes\hat{\boldsymbol{k}}_1\}_2+\{\hat{\boldsymbol{k}}_2\otimes\hat{\boldsymbol{k}}_2\}_2]+g^{-}[\{\hat{\boldsymbol{k}}_1\otimes\hat{\boldsymbol{k}}_1\}_2-\{\hat{\boldsymbol{k}}_2\otimes\hat{\boldsymbol{k}}_2\}_2]+g_s\{\hat{\boldsymbol{k}}_1\otimes\hat{\boldsymbol{k}}_2\}_2+g_0\{[\hat{\boldsymbol{k}}_1\times\hat{\boldsymbol{k}}_2]\otimes[\hat{\boldsymbol{k}}_1\times\hat{\boldsymbol{k}}_2]\}_2. \tag{4}$$

The monopole amplitude is represented by a scalar $\boldsymbol{A}_0\equiv g_m$. Using the tensorial product properties [13], Eqs. (3) and (4) can be simplified to the following form [14]:

$$M+Q=f_1(\hat{\boldsymbol{k}}_1\cdot\hat{\boldsymbol{e}})^2+f_2(\hat{\boldsymbol{k}}_2\cdot\hat{\boldsymbol{e}})^2+f_s(\hat{\boldsymbol{k}}_1\cdot\hat{\boldsymbol{e}})(\hat{\boldsymbol{k}}_2\cdot\hat{\boldsymbol{e}})+f_0(\hat{\boldsymbol{e}}\cdot\hat{\boldsymbol{e}}), \tag{5}$$

where the set of amplitudes in Eq. (5) is expressed via the amplitudes introduced in Eq. (4) as

$$f_1=g^{+}+g^{-}-g_0,\quad f_2=g^{+}-g^{-}-g_0,$$

$$f_s=g_s+2xg_0,\quad f_0=-\frac{2}{3}g^{+}-\frac{x}{3}g_s+\frac{2}{3}(1-x^2)g_0+g_m. \tag{6}$$

Here we use a shortcut $x\equiv\cos\theta_{12}$.

In this Brief Report, we demonstrate that complexity of the TPDI leads to the phenomenon of two distinct correlated escape modes: one is associated with the center-of-mass motion of the photoelectron pair whereas another is related to their relative motion. The kinematical factor associated with the center-of-mass motion favors a large total momentum of

*Electronic address: A.Kheifets@anu.edu.au
†Electronic address: I.Bray@murdoch.edu.au

the pair $\boldsymbol{p}=\boldsymbol{k}_1+\boldsymbol{k}_2$ which is gained at the parallel escape. In contrast, the kinematics of the relative motion mode favors a large relative momentum $\boldsymbol{k}=\boldsymbol{k}_1-\boldsymbol{k}_2$ which is maximized at the antiparallel escape. The dynamical correlation factor which is governed by the interelectron repulsion peaks strongly at the antiparallel emission in both modes. However, the width of this factor is much wider in the relative motion mode as compared to the center-of-mass mode. This can be explained by lesser interelectron repulsion in the former mode as compared to the latter.

In the following, we restrict ourselves to only the quadrupole amplitude and concentrate on the kinematics where the quadrupole channel is either the sole contributor to the TPDI or strongly dominant over the monopole channel. For simplicity, we consider the equal-energy-sharing kinematics $E_1=E_2$. We rewrite Eq. (4) with respect to the Jacobian momenta as

$$\boldsymbol{A}_2 = g_k\{\hat{\boldsymbol{k}}\otimes\hat{\boldsymbol{k}}\}_2 + g_p\{\hat{\boldsymbol{p}}\otimes\hat{\boldsymbol{p}}\}_2 + g_{kp}\{[\hat{\boldsymbol{k}}\times\hat{\boldsymbol{p}}]\otimes[\hat{\boldsymbol{k}}\times\hat{\boldsymbol{p}}]\}_2, \tag{7}$$

where

$$g_k = \frac{1}{4}(2g^+ - g_s), \quad g_p = \frac{1}{4}(2g^+ + g_s), \quad g_{kp} = \frac{1}{4}g_0, \tag{8}$$

and $\hat{\boldsymbol{p}}=\boldsymbol{p}/p$ and $\hat{\boldsymbol{k}}=\boldsymbol{k}/k$. Using similar notations, the dipole amplitude of SPDI (1) under the equal-energy-sharing condition is parametrized as $D\propto f_p(\hat{\boldsymbol{p}}\cdot\hat{\boldsymbol{e}})$, $f^+\equiv f_p$, $f^-=0$. We note that D is *linear* with respect to $\hat{\boldsymbol{p}}$ and does not contain $\hat{\boldsymbol{k}}$ under the equal energy condition. In contrast, Q is *quadratic* with respect to $\hat{\boldsymbol{k}}$ and $\hat{\boldsymbol{p}}$ and contains both vectors even when $E_1=E_2$. The amplitude g_k which enters Eq. (7) with the tensorial product $\{\hat{\boldsymbol{k}}\otimes\hat{\boldsymbol{k}}\}_2$ can be associated with the relative motion of the photoelectron pair described by the vector $\boldsymbol{k}$. Similarly, the amplitudes g_p can be associated with the center-of-mass motion and the amplitude g_{kp} which is entering Eq. (7) with the vector product $\hat{\boldsymbol{k}}\times\hat{\boldsymbol{p}}$ can be associated with the mixed motion mode.

To calculate amplitudes (8), we employed here the same dynamical model as was outlined in our previous work [12]. In this model, the electron-photon interaction was treated in the lowest-order perturbation theory using the closure approximation whereas the electron-electron interaction was included in full using the convergent close-coupling (CCC) method. The model proved to be capable of describing the angular correlation pattern in the two-electron continuum in good agreement with nonperturbative, with respect to the electromagnetic interaction, calculations [15,16].

We calculated amplitudes (8) in a range of excess energies E_1+E_2 from 1 eV to 20 eV above the double-ionization threshold. We employed a fairly large CCC basis set composed typically of $25-l$ box-space target states [17] with $0\leqslant l\leqslant 6$. Convergence of the calculation with respect to the basis size was thoroughly tested.

In the whole excess energy range, the amplitude g_{kp} was found insignificant as compared with g_k and g_p. The latter amplitudes were fitted with the Gaussian ansatz (2). A typical quality of the fit can be judged from Fig. 1 where the amplitudes g_k and g_p are exhibited for $E_1=E_2=2$ eV. The corresponding width parameters $\Delta\theta_{12}$ are plotted in Fig. 2, as a function of energy, along with the width parameter of the dipole amplitude f_p.

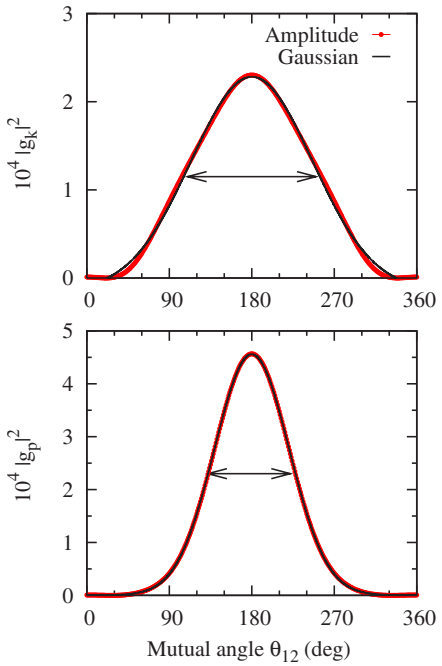

FIG. 1. (Color online) The TPDI amplitudes in the quadrupole channel g_k (top) and g_p (bottom) fitted with the Gaussian ansatz (2). The excess energy of 4 eV is shared equally between the photoelectrons $E_1=E_2=2$ eV. The arrows indicate the Gaussian width parameter $\Delta\theta_{12}$.

Across the energy range studied here, we observe a systematically larger Gaussian width of the relative motion amplitude g_k as compared with the center-of-mass motion amplitudes g_p and f_p, the latter two having a very similar width. We interpret this stark difference in terms of the strength of the electron-electron repulsion. This strength is much larger in the center-of-mass motion whose kinematics favors large p and hence the parallel emission as opposed to the relative

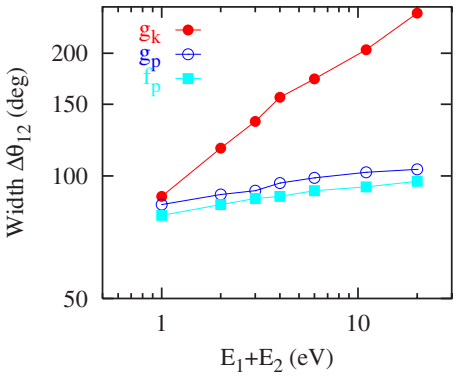

FIG. 2. (Color online) The Gaussian width parameters $\Delta\theta_{12}$ of the amplitudes g_k (red solid circles), g_p (blue open circles), and f_p (blue solid squares) as functions of the excess energy E_1+E_2. Extraction of the width parameters is illustrated in Fig. 1 for $E_1=E_2=2$ eV.

motion mode in which both the kinematic and dynamical correlation factors favor large k associated with the antiparallel emission. We note that the mixed-mode amplitude is typically an order of magnitude smaller than the pure-mode amplitudes g_k and g_p, thus supporting our notion of distinct escape modes.

Parametrization (5) can also be rewritten with respect to the Jacobian momenta:

$$M + Q = f_p(\hat{\boldsymbol{p}} \cdot \hat{\boldsymbol{e}})^2 + f_k(\hat{\boldsymbol{k}} \cdot \hat{\boldsymbol{e}})^2 + f_{kp}(\hat{\boldsymbol{p}} \cdot \hat{\boldsymbol{e}})(\hat{\boldsymbol{k}} \cdot \hat{\boldsymbol{e}}) + f_0(\hat{\boldsymbol{e}} \cdot \hat{\boldsymbol{\epsilon}}), \tag{9}$$

where

$$f_p = \frac{1}{4}(f_1 + f_2 + f_s), \quad f_k = \frac{1}{4}(f_1 + f_2 - f_s),$$

$$f_{kp} = \frac{1}{2}(f_1 - f_2) = 0 \quad \text{for } E_1 = E_2. \tag{10}$$

However, all the amplitudes f_k, f_p, and f_0 have generally the same Gaussian width which is in between the relative motion width and the center-of-mass width indicated in Fig. 2. Thus, parametrizations (5) and (9), which appear to be more concise and practical, do not reveal a clear mode separation.

For illustration, we consider two kinematics where these properties of the quadrupole amplitude can be studied experimentally. First, we consider TPDI with linearly polarized light $\hat{\boldsymbol{e}} = \hat{\boldsymbol{\epsilon}}$ where $\hat{\boldsymbol{\epsilon}}$ indicates the direction of the major axis of the polarization ellipse. Taking this direction as the quantization axis z and detecting both electrons in the polarization plane (the so-called coplanar kinematics), we can write the quadrupole amplitude as

$$\begin{aligned} Q &= g_k\left[(\cos\theta_1 - \cos\theta_2)^2 - \frac{2}{3}(1-x)\right] \\ &\quad + g_p\left[(\cos\theta_1 + \cos\theta_2)^2 - \frac{2}{3}(1+x)\right] + \frac{1}{3}g_{kp}(x^2-1) \\ &\equiv f_k(\cos\theta_1 - \cos\theta_2)^2 + f_p(\cos\theta_1 + \cos\theta_2)^2 + f_0. \end{aligned} \tag{11}$$

From these equations, it is seen that the amplitudes g_p and g_k contribute quite differently to the corresponding matrix elements. Both amplitudes peak strongly near $\theta_{12} = 180^\circ$. However, the kinematic factor corresponding to g_p has a node at this angle whereas the kinematic factor accompanying g_k has a peak. As a result, the term proportional to g_k dominates strongly the quadrupole amplitude. This dominance is illustrated in the top panel of Fig. 3 where the triply differential cross section (TDCS) $d\sigma/dE_1 d\Omega_1 d\Omega_2$ of the TPDI of He at $E_1 = E_2 = 2$ eV and the coplanar kinematics is plotted as a function of the variable escape angle θ_2 and fixed escape angle $\theta_1 = 0^\circ$. Three calculations are displayed in the figure. The first TDCS is generated from the sum of the monopole and quadrupole amplitudes $d\sigma/dE_1 d\Omega_1 d\Omega_2 \propto |M+Q|^2$ (dotted line). The second is obtained from the quadrupole amplitude alone, $d\sigma/dE_1 d\Omega_1 d\Omega_2 \propto |Q|^2$ (solid line). In the third calculation, a restricted quadrupole amplitude is used, $d\sigma/dE_1 d\Omega_1 d\Omega_2 \propto |Q(g_k)|^2$, in which the only g_k contribution is retained (solid circles).

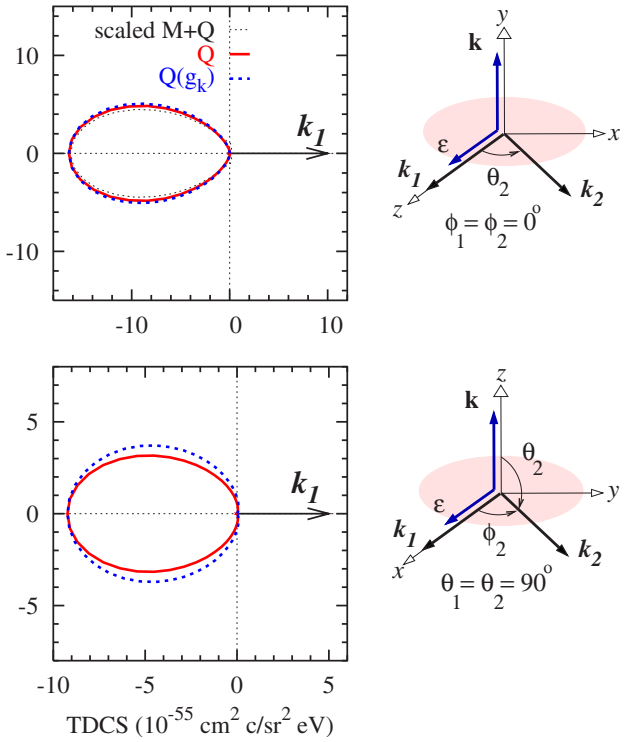

FIG. 3. (Color online) Triply differential cross section $d\sigma/dE_1 d\Omega_1 d\Omega_2$ of the TPDI of He at $E_1 = E_2 = 2$ eV. Top: linear polarization and coplanar geometry $\phi_1 = \phi_2 = 0$; one electron is fixed along the polarization axis of light $\theta_1 = 0$, and the TDCS is plotted as a function of the variable escape angle of another electron θ_2. The thin black dotted line corresponds to the sum of the monopole and quadrupole amplitudes $\propto |M+Q|^2$. The red solid line corresponds to the quadrupole amplitude alone $\propto |M|^2$ whereas the blue thick dotted line exhibits the contribution of the $\propto |M(g_k)|^2$ term only. The black dotted curve is scaled to the red solid curve at its maximum by a factor of 0.73 Bottom: circular polarization and perpendicular geometry $\theta_1 = \theta_2 = 90$; one electron is fixed along the direction of the photon propagation $\phi_1 = 0$, and the TDCS is plotted as a function of the variable escape angle of another electron ϕ_2.

To make a shape comparison, the first TDCS is scaled to the second by applying a scaling factor of 0.73. No further scaling is applied between the second and third TDCS's. We see that, indeed, the main features of the TDCS's originate from the quadrupole amplitude alone and the role of the monopole amplitude is insignificant in this geometry. By comparing the second and third TDCS's, we elucidate the dominance of the g_k term which persists at all fixed angles θ_1. It is particularly strong at a fixed escape angle $\theta_1 = 0$ when nearly all the contribution to the quadrupole amplitude comes from the g_k term.

For the second illustration, we take the case of circularly polarized light $\hat{\boldsymbol{e}} = (\hat{\boldsymbol{\epsilon}} + i\hat{\boldsymbol{\zeta}})/\sqrt{2}$ where $\hat{\boldsymbol{\zeta}} = \hat{\boldsymbol{k}} \times \hat{\boldsymbol{\epsilon}}$ and $\hat{\boldsymbol{k}}$ indicates the direction of the photon wave vector. We direct the z axis along $\hat{\boldsymbol{k}}$ and again detect electrons in the polarization plane. The quadrupole amplitude for this complanar geometry becomes

$$Q = 2e^{i(\phi_1+\phi_2)}\left[g_p \cos^2 \frac{\phi_{12}}{2} - g_k \sin^2 \frac{\phi_{12}}{2} \right]$$

$$\equiv \frac{1}{2} f_k [e^{i\phi_1} - e^{i\phi_2}]^2 + \frac{1}{2} f_p [e^{i\phi_1} + e^{i\phi_2}]^2 + f_0. \quad (12)$$

Here we introduced $\phi_{12} \equiv \phi_1 - \phi_2$. The corresponding TDCS for the same equal energy sharing $E_1 = E_2 = 2$ eV is shown on the bottom panel of Fig. 3. We see again a strong dominance of the g_k term as the corresponding kinematic factor peaks at $\phi_1 - \phi_2 = 180^\circ$ where g_k has peak as well. On the contrary, the kinematic factor accompanying g_p has a node at $\phi_1 - \phi_2 = 180^\circ$. We note that the monopole amplitude is zero for TPDI with 100% circularly polarized light at any geometry since it cannot accommodate two units of angular momentum projection.

We have to note that it is the parametrization of the quadrupole amplitude with respect to the Jacobian momenta (7) and (8) that gives such a clear separation of the center-of-mass and relative motion modes. Our earlier attempt in Ref. [12] to apply the Gaussian ansatz (2) showed no such a clear systematic behavior of the angular correlation width with respect of the excess energy as exhibited in Fig. 2.

Comparing two different parametrizations of TPDI introduced in our earlier work [12] and, later, in Ref. [14], one may notice a fewer number of independent amplitudes (4 instead of 5) in the latter. However, the present parametrization has advantage at certain kinematics. For instance, only two amplitudes are needed instead of three in the case of circularly polarized light [see Eq. (12)].

In conclusion, we demonstrated the presense of two distinct photoelectron escape modes in the quadrupole channel of two-photon double ionization of He. One of the modes corresponds to the center-of-mass motion of the photoelectron pair. The kinematics of this mode enhances the total momentum of the pair and therefore favors the parallel emission. The interelectron repulsion is strong in this mode, and the angular correlation width is relatively small. In the other, relative motion, mode the kinematic factor enhances the relative momentum of the pair and therefore favors the antiparallel emission. The interelectron repulsion is much weaker in this mode, and the angular correlation width is much larger. Both modes are fully symmetric and present under the equal-energy-sharing condition. In contrast, the single-photon double ionization has only one fully symmetric mode which is associated with the center-of-mass motion. This mode, in terms of the angular correlation width, is very similar to the center-of-mass motion mode in two-photon double ionization. The presense of two modes is a reflection of the quadratic tensorial structure of the quadrupole photoionization amplitude as compared to the linear structure of the dipole photoionization amplitude.

The outlined effect can be observed experimentally. For TPDI with linearly polarized light, the quadrupole amplitude dominates the cross section at the coplanar kinematics when one of the photoelectrons is aligned with the direction of the polarization axis of light. The quadrupole amplitude is the sole contributor to the TPDI with the circularly polarized light. In both cases, nearly all the TPDI yield is associated with the relative motion of the photoelectrons. Although the contribution of the center-of-mass mode is generally small, it can still be detected by observing the recoil ion which absorbs the total momentum of the photoelectron pair.

The area of excess energies below 1 eV above the threshold has not been investigated in the present study due to prohibitively slow convergence with respect to the photoelectron angular momenta. Figure 2 indicates that different modes tend to converge near the threshold. More study is needed to resolve this issue.

The authors wish to thank the Australian Partnership for Advanced Computing (APAC) and ISA Technologies, Perth, Western Australia, for provision of their computing facilities. Support of the Australian Research Council in the form of Discovery Grant No. DP0451211 is acknowledged.

[1] J. Ullrich *et al.*, Rep. Prog. Phys. **66**, 1463 (2003).
[2] J. S. Briggs and V. Schmidt, J. Phys. B **33**, R1 (2000).
[3] G. C. King and L. Avaldi, J. Phys. B **33**, R215 (2000).
[4] L. Avaldi and A. Huetz, J. Phys. B **38**, S861 (2005).
[5] A. Huetz, P. Selles, D. Waymel, and J. Mazeau, J. Phys. B **24**, 1917 (1991).
[6] L. Malegat, P. Selles, and A. Huetz, J. Phys. B **30**, 251 (1997).
[7] A. R. P. Rau, J. Phys. B **9**, L283 (1976).
[8] J. M. Feagin, J. Phys. B **17**, 2433 (1984).
[9] A. S. Kheifets and I. Bray, Phys. Rev. A **65**, 022708 (2002).
[10] P. Bolognesi *et al.*, J. Phys. B **36**, L241 (2003).
[11] A. Knapp *et al.*, J. Phys. B **28**, 645 (2005).
[12] A. S. Kheifets and I. A. Ivanov, J. Phys. B **38**, 471 (2006).
[13] D. A. Varshalovich, *Quantum Theory of Angular Momentum*, 1st ed. (World Scientific, Philadelphia, 1988).
[14] Y. A. Istomin *et al.*, Phys. Rev. Lett. **97**, 123002 (2006).
[15] J. Colgan and M. S. Pindzola, Phys. Rev. Lett. **88**, 173002 (2002).
[16] S. X. Hu, J. Colgan, and L. A. Collins, J. Phys. B **38**, L35 (2005).
[17] I. Bray, K. Bartschat, and A. T. Stelbovics, Phys. Rev. A **67**, 060704(R) (2003).